CHAPTER-4

TRIBOLOGICAL BEHAVIOUR OF TEXTURED DISC IN DRY CONDITION

The following chapter presents the results on the characterisation of the material and textures and the tribological behaviour of steel under dry sliding. The chapter begins with the presentation of results on the characterisation of AISI52100 bearing steel and textures. This is followed by the results on the friction and wear behaviour of untextured and textured specimens at different loads and speeds under dry sliding condition. The results have been discussed to understand the effect of the shape and density of textures on the friction and wear performance of steel and the dominating mechanisms of wear have been highlighted.

4.1 RESULTS

4.1.1 CHEMICAL COMPOSITION OF AISI52100

The chemical composition of the bearing steel, as analysed through energy-dispersive X-ray spectroscopy, has been given in Table 4.1.

Table 4.1 Chemical composition of bearing steel (wt. %).

C	Cr	Ni	Mn	Si	Fe
1.00	1.40	0.23	0.50	0.20	96.67

4.1.2 CHARACTERIZATION OF LASER TEXTURED SURFACE

A laser textured disc and a pin are presented in Fig. 4.1. The textured disc has circular dimples with 7% density.

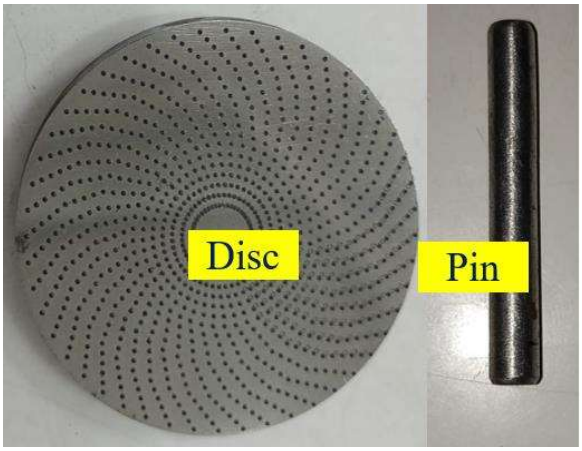

Fig. 4.1 Laser textured disc and a pin.

Figure 4.2 (a through d) shows the optical micrographs of the laser-textured surfaces of the bearing steel discs with different dimple densities. The laser textured disc surfaces having circular dimples with 7% and 20% densities are given in Fig. 4.2 (a) and (b), respectively. A variation in the spacing between regularly formed dimples and hence, the variation in the density of dimples can be clearly observed from the figure. The same can be observed for bi-triangular dimples with 7% and 20% densities in Fig. 4.2 (c) and (d), respectively. The spacing between dimples is more in the case of 7% dimples in comparison to 20% dimples. Also, the spacing between the dimples along the spiral is the same in respective texturing; however, the spacing changes from one spiral to others if seen from centre to circumference, as illustrated in Fig. 4.2 (a through d).

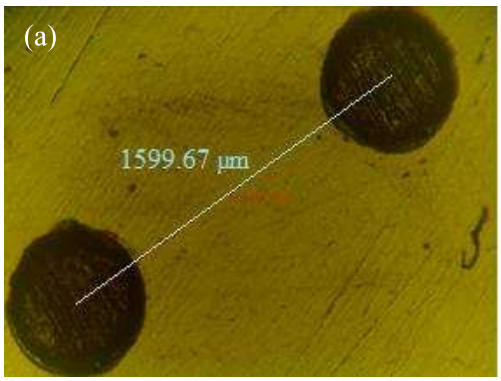

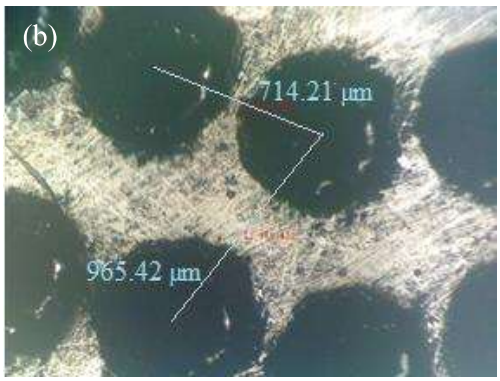

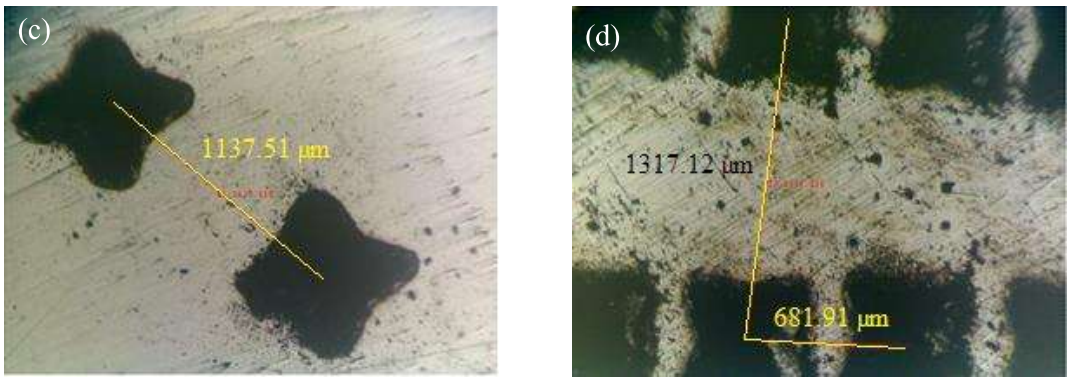

Fig. 4.2 Optical micrographs of laser textured surface of steel discs having (a)7% density of circular dimples (CT7), (b) 20% density of circular dimples (CT20), (c)7% density of bi-triangular dimples (BT7) and (d) 20% density of bi-triangular dimples (BT20).

Sample designation and various parameters of the dimples on the laser-textured discs are presented in Table 4.2.

Table. 4.2 Sample designation and dimple features

Sample Designation	Dimples	Area Density	Size (*d* or *l*), µm	Average Depth, µm	Distance in the array, µm
UT	Untextured	-	-	-	-
CT7	Circular	7%	500	8	1599.67
CT20	Circular	20%	500	8	714.21
BT7	Bi-triangular	7%	500	8	1137.51
BT20	Bi-triangular	20%	500	8	681.91

Figure 4.3 (a) and (c) show the micrographs of bi-triangular and circular dimples, respectively, whereas Fig. 4.3 (b) and (d), respectively, show the profile of the circular and bi-triangular dimples as detected by an optical profilometer. The micro dimples are about 500 µm in diameter and about 8 µm in depth.

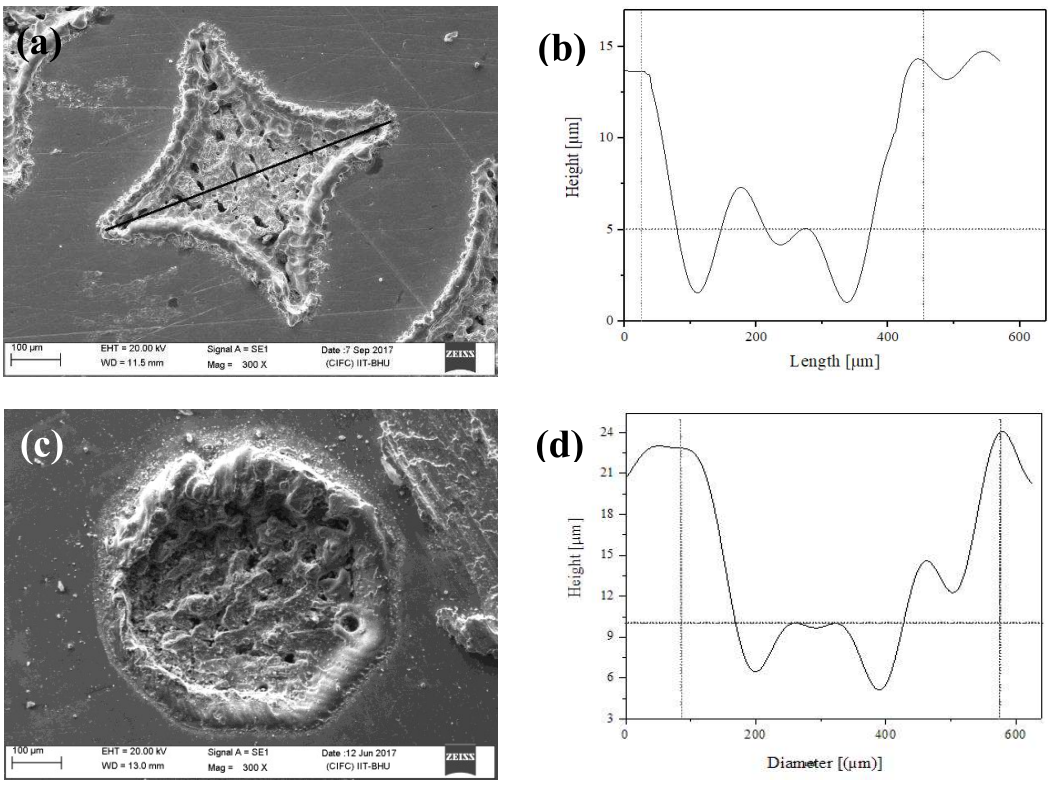

Fig. 4.3 SEM micrograph (a, c) and 2D profile illustrating the lengths, average depth and height of micro-pores (b, d).

The dimples have typical bulges or burrs around their rim. Due to the high-energy action of the laser, the metal is partially melted and sputtered metal is deposited on the brim of the dimples, resulting in the creation of the bulge, as shown in Fig. 4.3 (c), which depicts the morphology of a single dimple. The bulges on the brim of micro-dimples may lead to an increase in initial roughness.

4.2 EFFECT OF LASER SURFACE TEXTURING ON THE FRICTION AND WEAR PROPERTIES

4.2.1 FRICTION BEHAVIOUR

Figure 4.4 demonstrates the variation of the coefficient of friction with a number of revolutions at 0.2 m/s and a constant load of 15 N. For all of the specimens, the variation

displays a typical fluctuating tendency. The coefficient of friction initially rises for 1500 revolutions and fluctuates thereafter around an average value for UT and BT7. The coefficient of friction remains constant with typical fluctuations for CT7 and BT20. However, it slightly drops for CT7 at around 3000 revolutions and follows the trend again. It can also be noted that the coefficient of friction for CT20 initially rises and suddenly drops to 0.4 at 7000 revolutions.

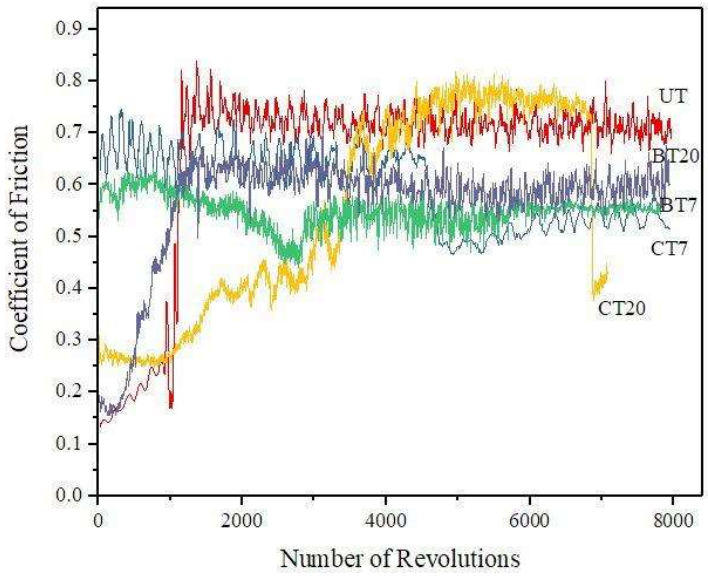

Fig. 4.4 Variation of coefficient of friction with the number of revolutions at a load of 15 N and speed of 0.2 m/s.

Figure 4.5 depicts the variation of the coefficient of friction with the number of revolutions at 0.6 m/s and a constant load of 15 N. For all of the specimens, the variation of coefficient of friction has a typical fluctuation, but the amplitude of variation is fairly small for BT20. The coefficient of friction for BT20 lowers after 4000 revolutions, while the coefficient of friction for CT20 drops near the end of the test. One may observe a decrease in the coefficient of friction of untextured (UT) disc after 6000 revolutions.

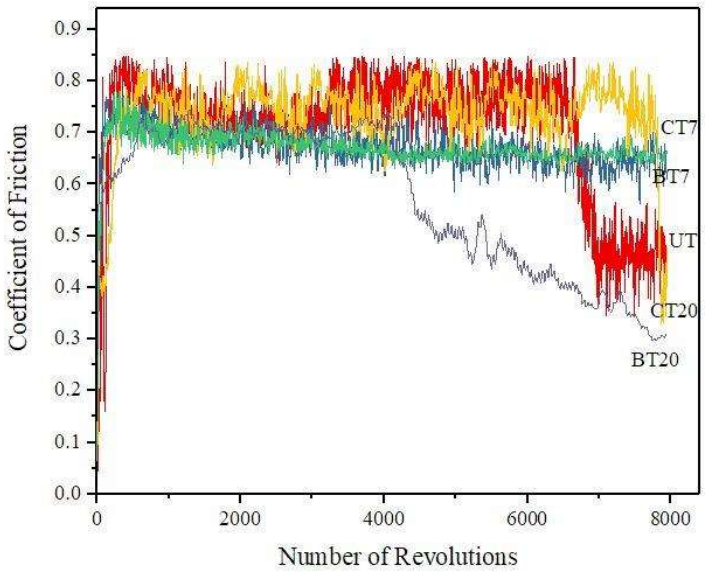

Fig. 4.5 Variation of coefficient of friction with the number of revolutions at a load of 15 N and speed of 0.6 m/s.

Figure 4.6 shows the variation of the coefficient of friction with a number of revolutions at 1 m/s and a constant load of 15 N. The variation reveals a typical fluctuating trend for all the specimens, but the amplitude of fluctuation is quite small for CT20 and BT20 in comparison to UT, CT7, and BT7. It can also be noted that the coefficient of friction drops suddenly from a value of 0.6 to 0.2 for CT20 after running about 2500 cycles and maintains this value until the full duration of the test. A similar fall in the value can be observed for BT7 after 5500 revolutions.

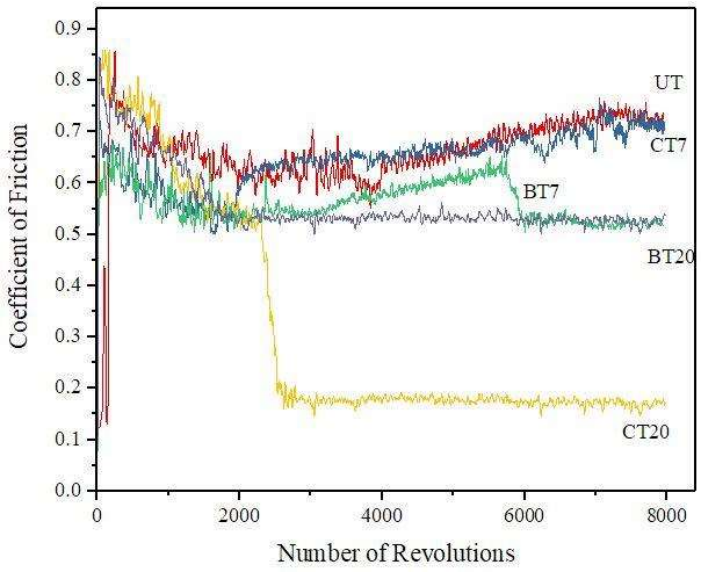

Fig. 4.6 Variation of coefficient of friction with the number of revolutions at a load of 15 N and speed of 1 m/s.

The variation of the coefficient of friction with the number of revolutions at a speed of 0.2 m/s and a constant load of 30 N is shown in Fig. 4.7. The variation in the coefficient of friction has normal fluctuation, which is slightly more in the case of CT7. It's also worth noting that the tests for BT20 and CT20 conclude at roughly 8000 revolutions, whereas the test could run for 6000 revolutions only for CT7, BT7 and UT, probably due to the increased chatter caused by the wearing of the pin at this speed and load.

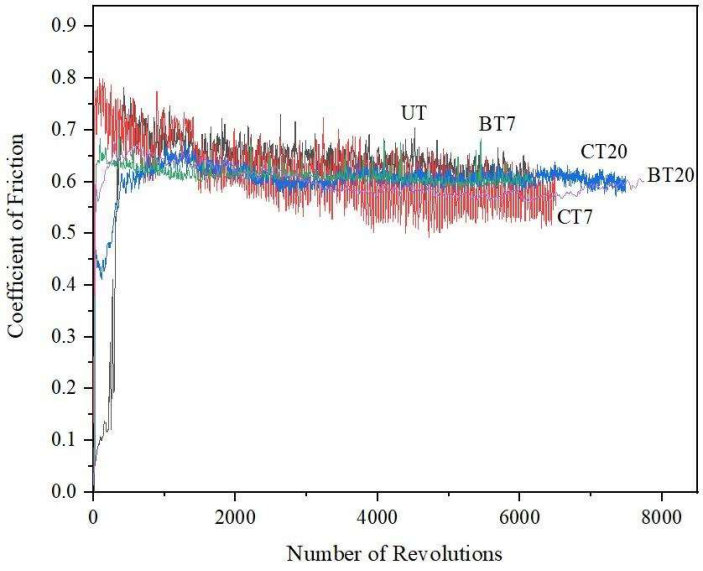

Fig. 4.7 Variation of coefficient of friction with the number of revolutions at a load of 30 N and speed of 0.2 m/s.

Figure 4.8 shows the variation of the coefficient of friction with the number of revolutions at a speed of 0.6 m/s and a constant load of 30 N. In comparison to other load and speed situations, all of the specimens show slightly higher fluctuation at this load and speed. In the case of UT, the coefficient of friction has an amplitude of variation from 0.45 to 0.77 for the first 2000 revolutions, which decreases to a range of 0.54 to 0.65 for the rest of the duration of the test. The maximum amplitude of variation for CT7 ranges from 0.54 to 0.71, with a premature end of the test near around 7000 revolutions. In the case of CT20, the coefficient of friction after an initial drop to 0.3 for about 250 revolutions rises to 0.6 after 500 revolutions and continues with typical fluctuation till the end of the test. BT7 has a value of 0.58 for roughly 900 revolutions, then drops to 0.55 after 3500 revolutions, but the average stays near 0.57 throughout the entire revolution. After an initial drop to 0.51 for 150 revolutions, the coefficient of friction in BT20 continues for the rest of the test with a value lying between 0.50 to 0.52.

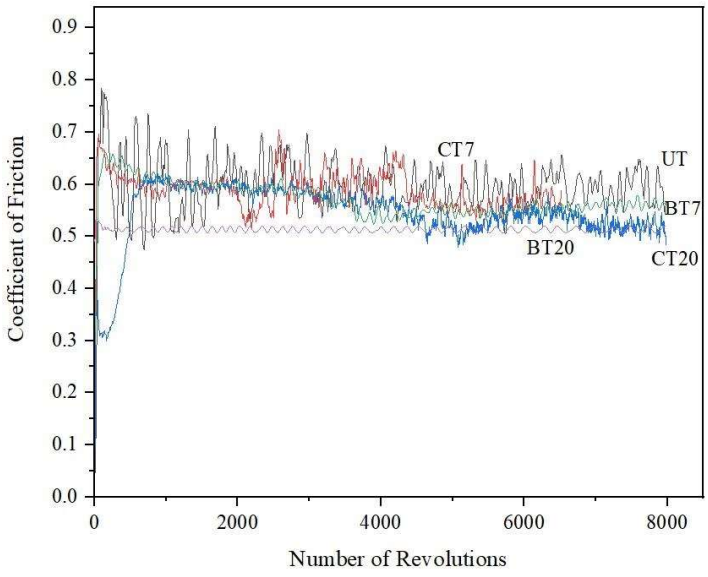

Fig. 4.8 Variation of coefficient of friction with the number of revolutions at a load of 30 N and speed of 0.6 m/s.

The variation of coefficient of friction with the number of revolutions at a speed of 1 m/s and a constant load of 30 N is presented in Fig. 4.9 for all the specimens used in the present study. The variation for all the specimens indicates that after roughly 1700 revolutions, the coefficient of friction becomes stable with some fluctuation throughout the test. In the case of UT, the average coefficient of friction is about 0.57, whereas the values are lower for the textured discs. The fluctuation in the value is marginal for the textured specimens, with an average of about 0.52.

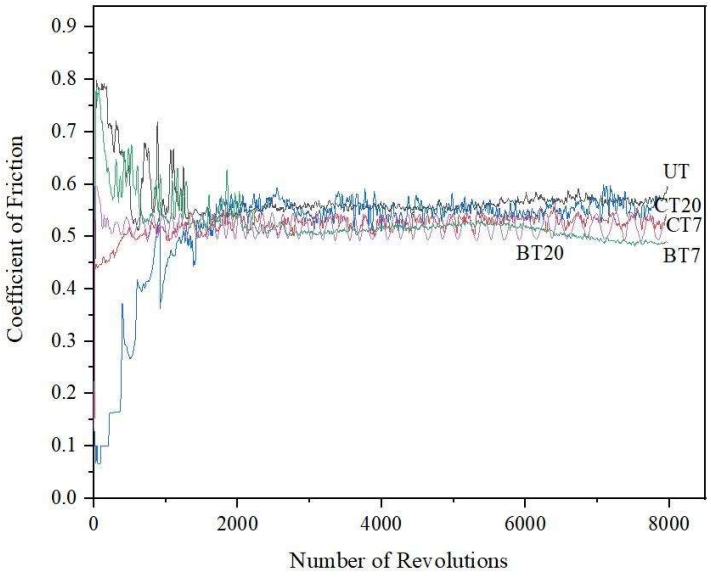

Fig. 4.9 Variation of coefficient of friction with the number of revolutions at a load of 30 N and speed of 1 m/s.

Figure 4.10 shows the variation of the average coefficient of friction for UT, CT7, CT20, BT7, BT20 at different sliding speeds and a constant load of 15 N. For all test specimens, the average coefficient of friction is the highest at 0.6 m/s and the lowest at 0.2 m/s, with the exception of untextured (UT) and BT20. At 1.0 m/s, the coefficient of friction appears to fall in between. However, one can observe the effect of density as well as the shape of the dimples. At the lowest speed of 0.2 m/s used in the present investigation, the coefficient of friction decreases after texturing with 7% density circular dimples and remains in the same band for CT20, and BT7 before increasing finally for BT20. A similar trend of variation could be observed for a speed of 0.6 m/s, except that a decrease in coefficient of friction is observed from BT7 to BT20. However, at the highest speed of 1.0 m/s, the coefficient of friction first increases as one moves from untextured to CT7 before decreasing continuously as one moves from CT7 to CT20 to BT7 to BT20, indicating thus, the effect of density as well as the shape on friction reduction.

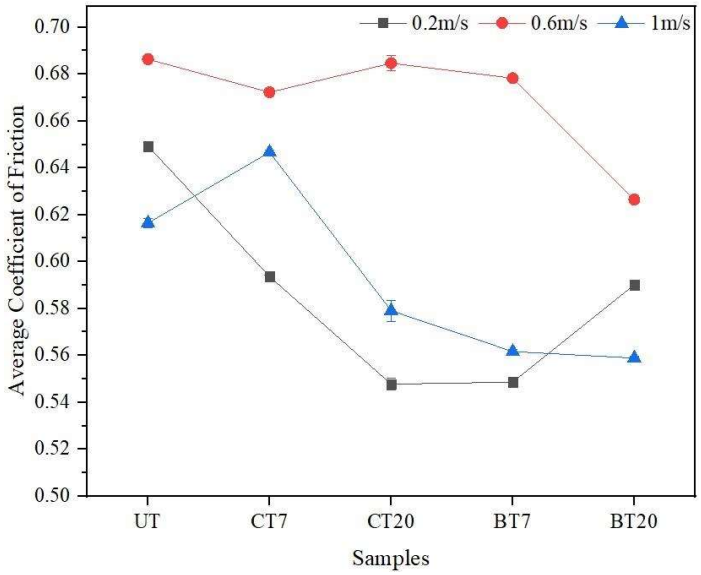

Fig. 4.10 Average coefficient of friction for various specimens at different speeds at a constant load of 15 N.

The average coefficient of friction for UT, CT7, CT20, BT7, and BT20 at different sliding speeds and a constant load of 30 N is shown in Fig. 4.11. For all test specimens, the average coefficient of friction is the highest at 0.2 m/s and the lowest at 1.0 m/s, with the exception of BT20. At the lowest speed of 0.2 m/s used in the present investigation, the coefficient of friction decreases after texturing with 20% density circular and bi-triangular dimples and remains in the same band for BT7 and CT7. A similar trend of variation could be observed for a speed of 0.6 m/s; however, a decrease in coefficient of friction is observed slightly more from CT7 to CT20 and BT7 to BT20. At the highest speed of 1.0 m/s, one may observe a sharp decrease in the coefficient of friction from UT to CT7. It may also be noticed that the coefficient of friction remains almost the same for the textured specimens at a speed of 1.0 m/s as evident from Fig. 4.11.

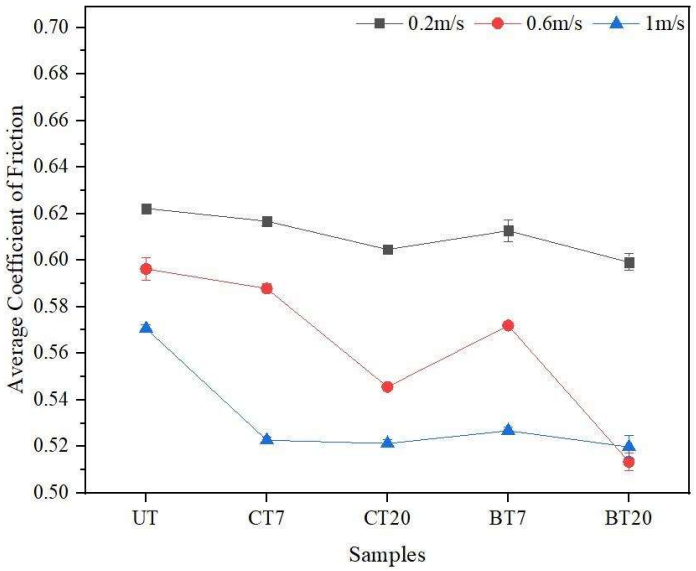

Fig.4.11 Average coefficient of friction for textured discs at different speeds and at a constant load of 30 N.

4.2.2 WEAR BEHAVIOUR

The wear rate for each specimen has been calculated by dividing the mass loss by the density of steel (taken as 7.81×10^3 kg/m^3). Figure 4.12 shows the variation of wear rate for untextured (UT) and textured specimens, namely, CT7, CT20, BT7, and BT20, having different densities and shapes at various sliding speeds of 0.2, 0.6, and 1.0 m/s and 15 N load. One could observe that textured specimens have less wear than the untextured sample at all the speeds used in the present study. It could further be seen from Fig. 4.12 that the wear rate either decreases or remains constant as one moves from CT7 to BT7 at speeds of 0.2 and 1.0 m/s, whereas the wear rate increases from CT20 to BT7 for a speed of 0.6 m/s. The wear rate is found to decrease from BT7 to BT20 as the speed changes from 0.6 and 1.0 m/s, whereas an increase could be observed for a speed of 0.2 m/s. A relatively more wear in the 7% circle density disc (CT7) may be due to the hard deposition on the surface surrounding the cavities. Also, the presence of microcavities is expected to entrap wear particles and minimize wear. In the case of the untextured disc, no such feature is present, and hence, a relative more loss of material. A higher wear of textured

disc with 20% bi-triangular dimples density (BT20) at 0.2 m/s may be because of the initial presence of deposited material and its subsequent wear.

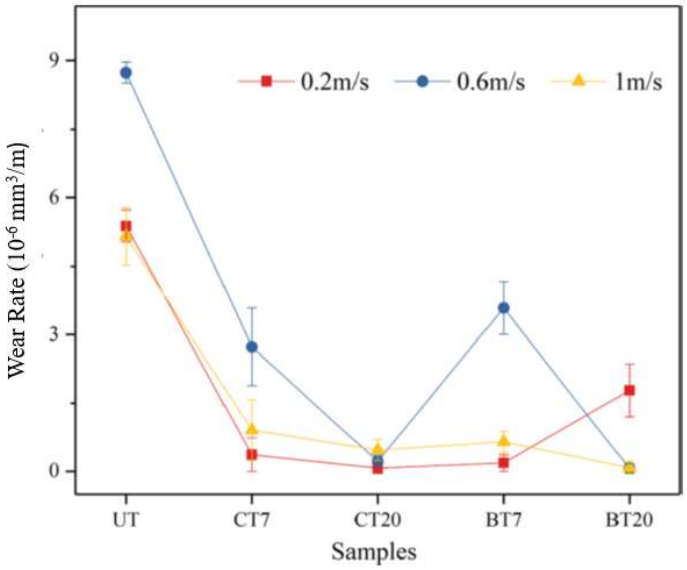

Fig. 4.12 Variation of wear rate in textured specimens at different speeds and at a constant load of 15 N.

The variation of wear rate for untextured (UT) and textured specimens, namely, CT7, CT20, BT7, and BT20 having different densities and shapes at various sliding speeds of 0.2, 0.6 and 1.0 m/s and a constant load of 30 N is presented in Fig. 4.13. At a speed of 0.2 m/s, the wear rate is found to decrease from UT to CT20 and remains almost constant till BT7 before increasing for BT20. However, the wear rate is observed to decrease as one moves from UT to BT7, followed by a slight increase thereafter for BT20 at sliding speeds of 0.6 and 1.0 m/s. The decrease is relatively steep in the case of 0.6 m/s than 1.0 m/s, as seen in Fig. 4.13.

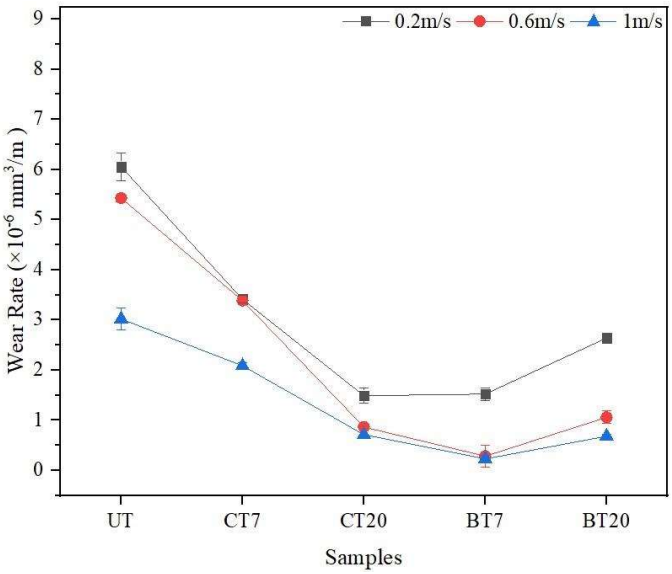

Fig.4.13 Variation of wear rate in textured specimens at different speeds and at a constant load of 30 N.

4.3 EXAMINATION OF WORN SURFACE

The worn surfaces of untextured and textured specimens have been examined under a scanning electron microscope to reveal the salient features. Figures 4.14 (a-e) show the morphologies of textured specimens as observed under a scanning electron microscope (SEM) at 0.2m/s and a constant load of 15 N. The worn surface of the untextured specimen shows a typical morphology of a worn steel surface with the presence of wear marks along the sliding direction and signs of adhesion. The worn surfaces of textured specimens show the presence of dimples along with wear tracks running parallel to the sliding direction. The dimples appear to be filled for CT7, CT20, and BT7 specimens, as seen from Figs. 4.14 (b, c, and d), whereas the bi-triangular dimples in BT20 have been observed to be still unfilled.

Figures 4.15 (a-e) present the morphologies of UT, CT7, CT20, BT7, and BT20 after sliding at a speed of 0.6 m/s and a constant load of 15 N. Similar features as observed for 0.2 m/s, could also be seen at a speed of 0.6 as evident from a comparison of Figs. 4.14 (a) and 4.15 (a) for the untextured surface. The textured surfaces show the presence of filled dimples

either completely (CT7 and BT7) or partially (CT20 and BT20) with wear debris at a speed of 0.6 m/s.

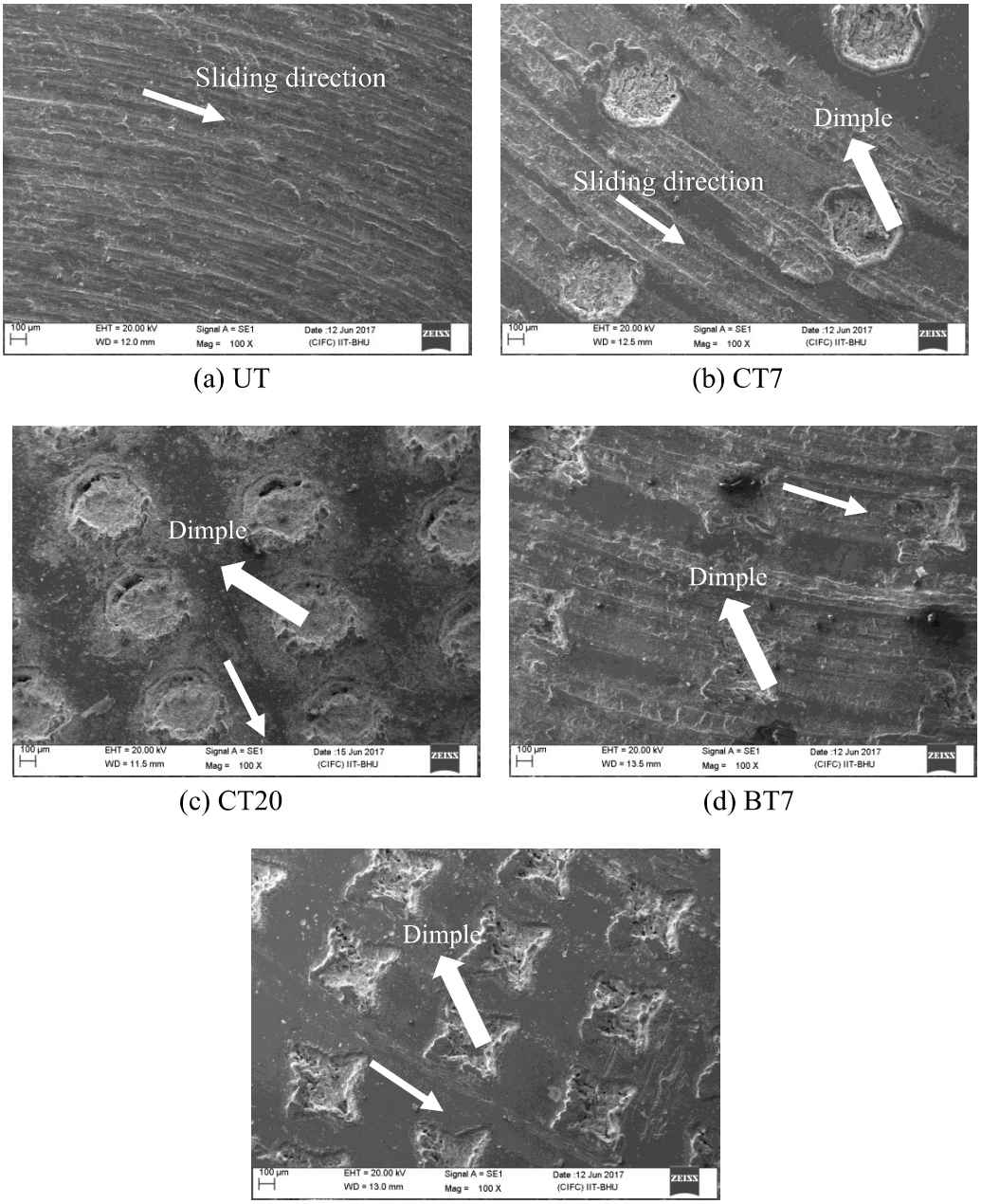

(a) UT (b) CT7

(c) CT20 (d) BT7

(e) BT20

Fig. 4.14 Scanning electron micrographs of worn surface of specimens after sliding under the dry condition at a load of 15 N and speed of 0.2 m/s.

.

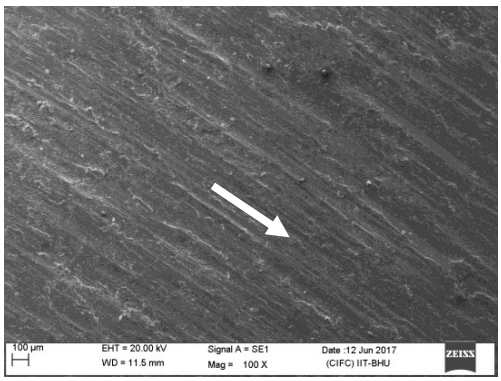

(a) UT

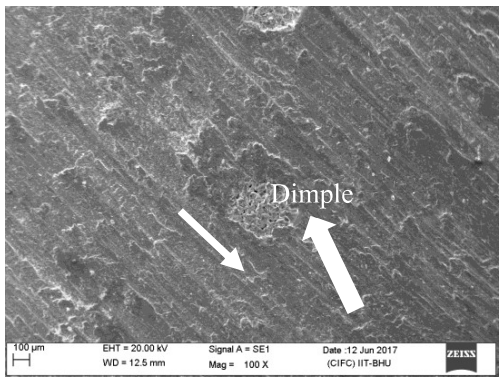

(b) CT7

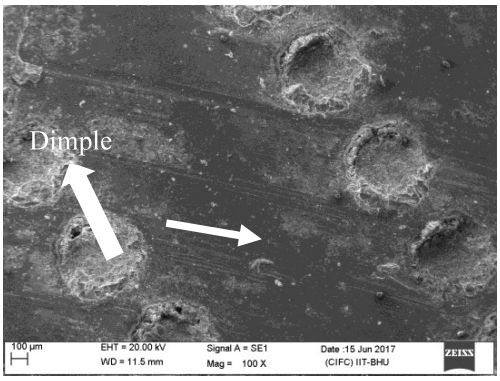

(c) CT20

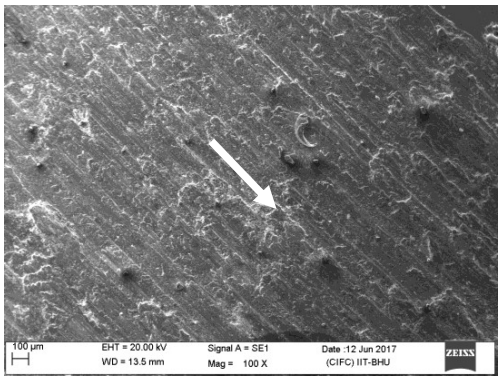

(d) BT7

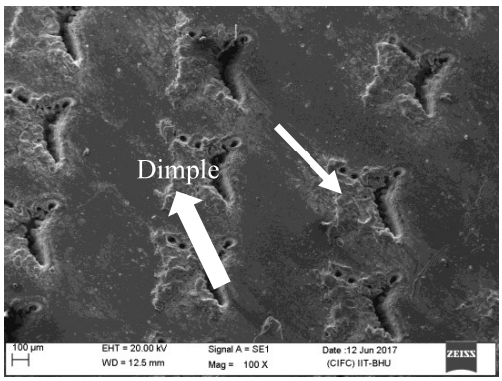

(e) BT20

Fig. 4.15 Scanning electron micrographs of worn surface of specimens after sliding under the dry condition at a load of 15 N and speed of 0.6 m/s.

The morphologies of UT, CT7, CT20, BT7, and BT20 after sliding at 1.0 m/s and a constant load of 15 N are shown in Figures 4.16. As can be seen from a comparison of Figs. 4.14 (a), 4.15 (a), and 4.16 (a) for the untextured surface, similar features as exhibited at 0.2

and 0.6 m/s are also be visible at 1.0 m/s. However, at 1.0 m/s, the surface appears to be covered by a compacted layer of oxide, which helps in inhibiting metal-metal contact and lowers the coefficient of friction by producing low-shear-strength junctions, as seen in Fig. 4.12. The surfaces also demonstrate the existence of dimples that are filled either entirely (BT7 and BT20) or partially (CT7 and CT20) with wear debris.

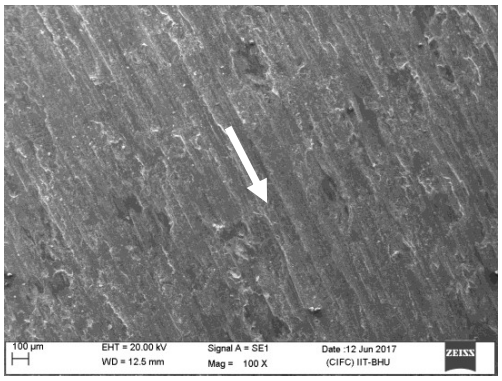

(a) UT

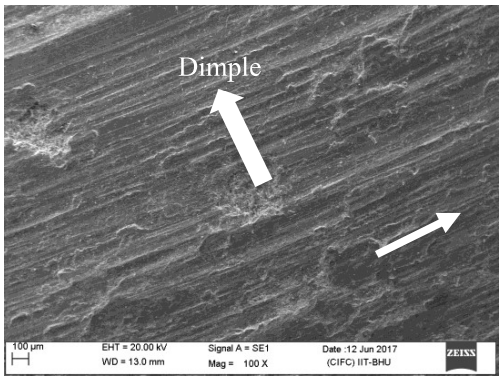

(b) CT7

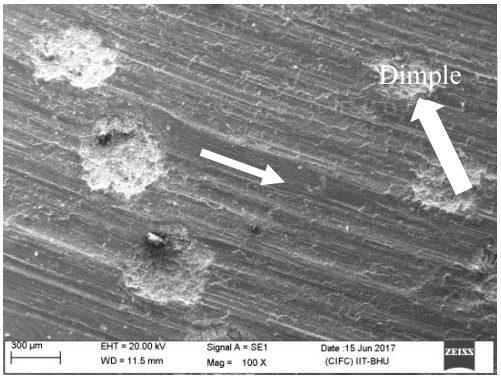

(c) CT20

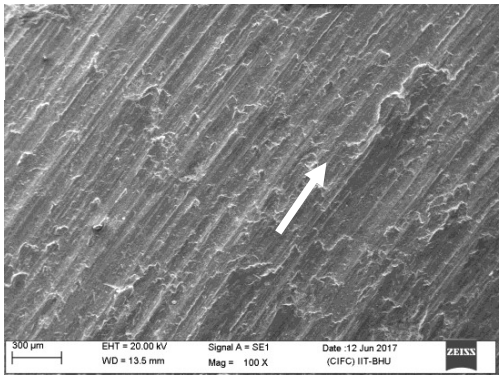

(d) BT7

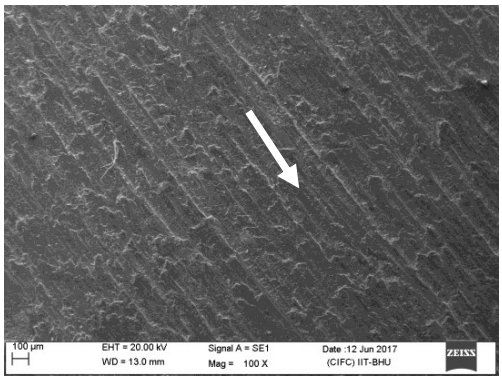

(e) BT20

Fig. 4.16 Scanning electron micrographs of worn surface of specimens after sliding under the dry condition at a load of 15 N and speed of 1 m/s.

The morphologies of textured materials as detected under a scanning electron microscope (SEM) at 0.2m/s and a constant load of 30 N are shown in Figs. 4.17 (a-e). The specimen's worn surface has a typical worn morphology of a steel surface, with wear markings along the sliding direction and traces of adhesion. Dimples and wear tracks running parallel to the sliding direction can be seen on the worn surfaces of textured specimens. As seen in Figs. 4.17 (b), the dimples in CT7 appear to be filled, whereas the dimples in CT20 and BT20 appear to be unfilled. The dimples on the surface of BT7 are filled with worn particles and show signs of adhesion.

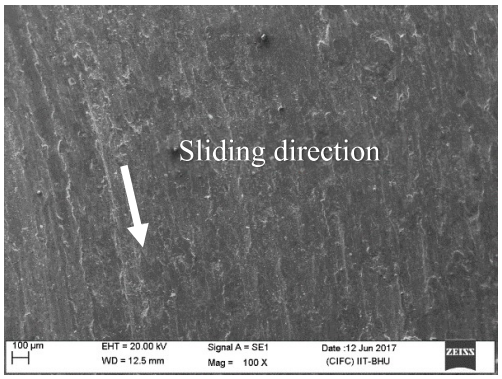

(a) UT

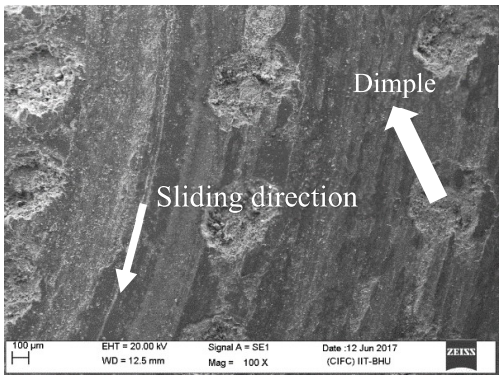

(b) CT7

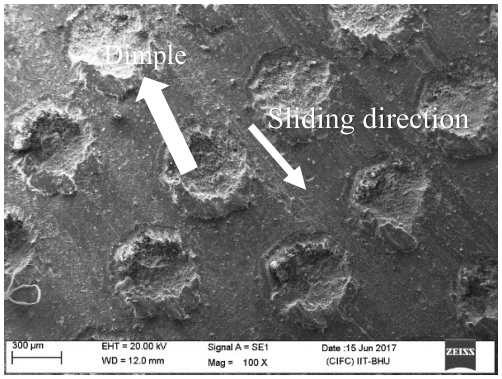

(c) CT20

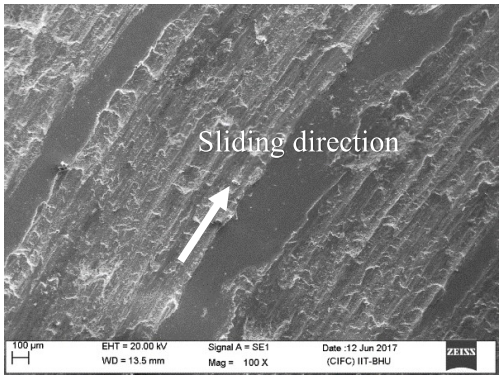

(d) BT7

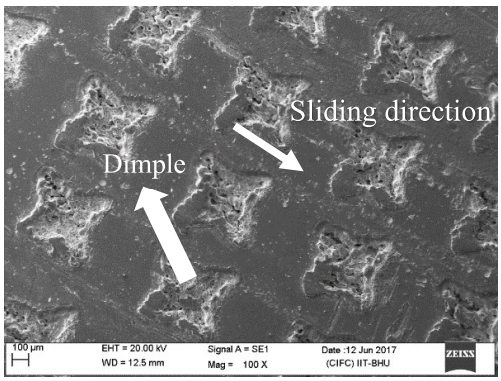

(e) BT20

Fig. 4.17 Scanning electron micrographs of worn surface of specimens after sliding under the dry condition at a load of 30 N and speed of 0.2 m/s.

The morphologies of UT, CT7, CT20, BT7, and BT20 after sliding at 0.6 m/s and a constant load of 30 N are shown in Figure 4.18. Similar features, as observed for 0.2 m/s, could also be seen at a speed of 0.6 m/s, as evident from a comparison of Figs. 4.17 and 4.18. At a speed of 0.6 m/s, the textured surfaces demonstrate the existence of dimples that are either entirely filled (CT7 or BT7) or partially filled (CT20 and BT20) with wear debris. However, the worn particles, in this case, remain present on the contact surface and form a transferred layer at the sliding interface as the speed increases. The formation of the transfer layer can be observed for CT7, CT20, BT7, and BT20.

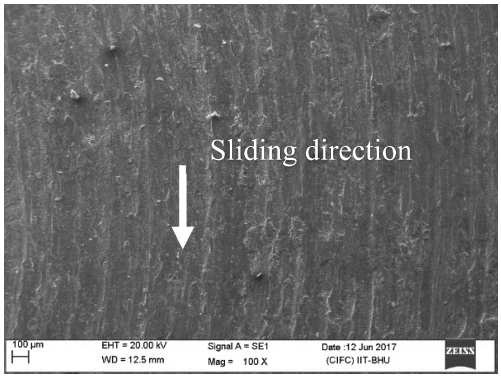

(a) UT

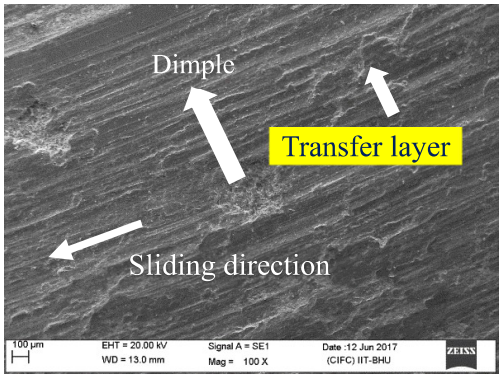

(b) CT7

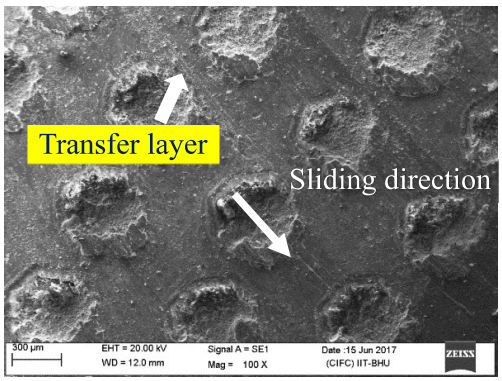

(c) CT20

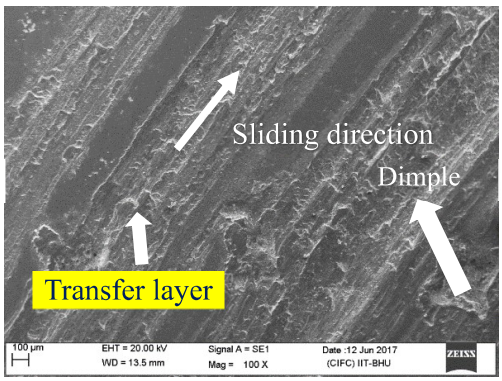

(d) BT7

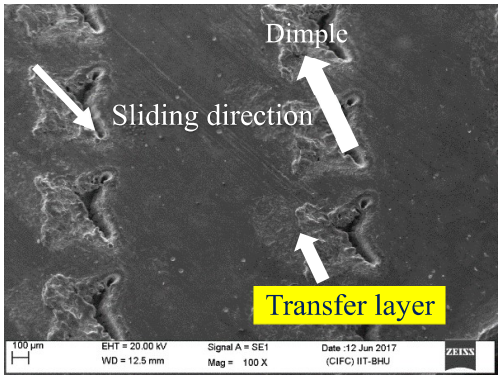

(e) BT20

Fig. 4.18 Scanning electron micrographs of worn surface of specimens after sliding under the dry condition at a load of 30 N and speed of 0.6 m/s.

Figures 4.19 illustrate the morphologies of UT, CT7, CT20, BT7, and BT20 after sliding at 1.0 m/s and a constant load of 30 N. As seen from Figs. 4.19 (c) and (e) corresponding to CT20 and BT20, respectively, the dimples appear to have filled to a greater extent, whereas, in the case of CT7 and BT7, the dimples have almost disappeared. At this load and speed, all surfaces, including the untextured (UT), have shown the presence of a compacted layer of wear debris with varying extent of compacted and area coverage.

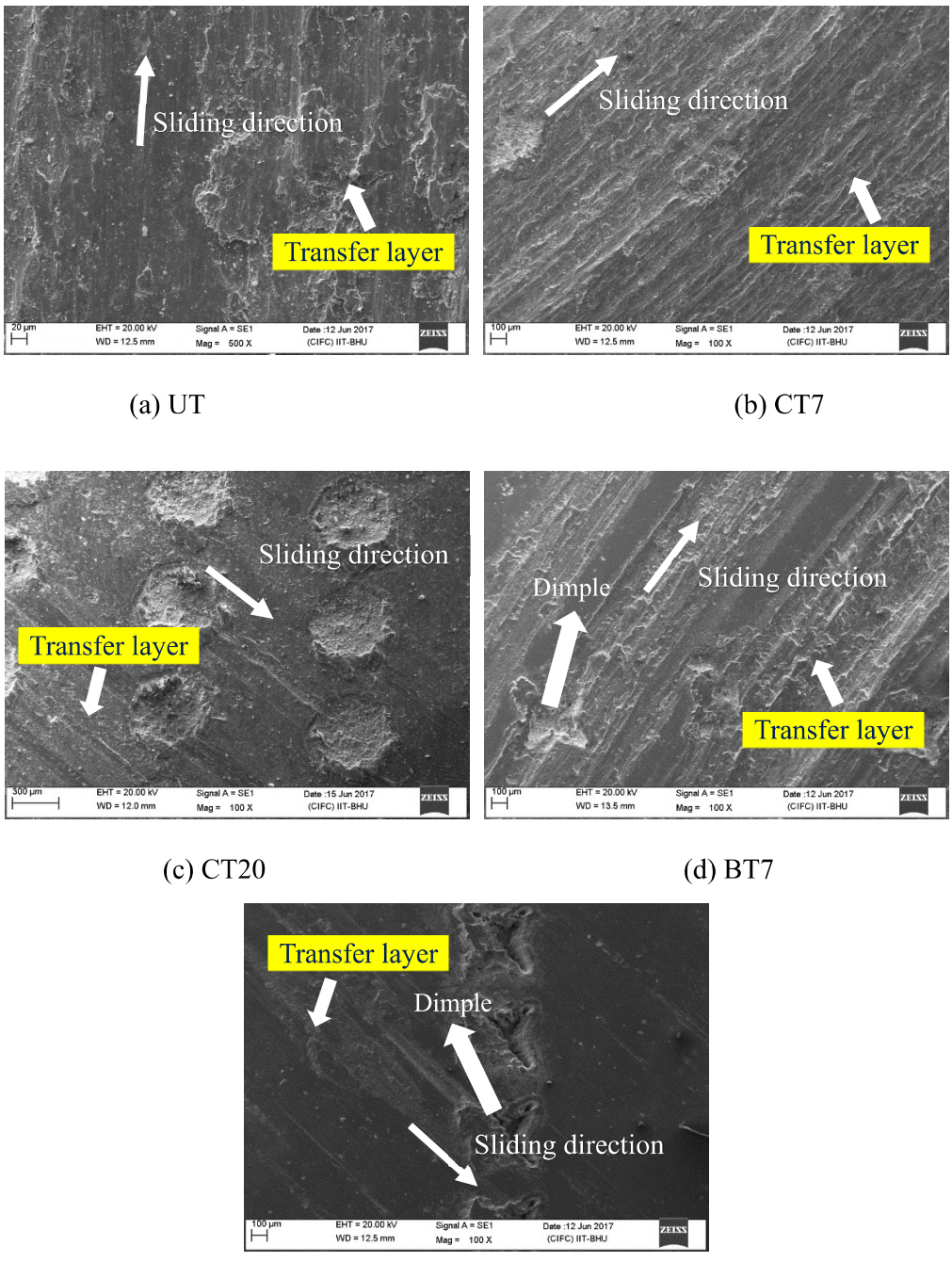

(a) UT (b) CT7

(c) CT20 (d) BT7

(e) BT20

Fig. 4.19 Scanning electron micrographs of worn surface of specimens after sliding under the dry condition at a load of 30 N and speed of 1 m/s.

Oxidation processes at contacts have been investigated by EDS (energy-dispersive X-ray spectroscopy). SEM image and EDS analysis of the worn surface of CT20 after sliding

under the dry condition at a constant load of 15 N and speed of 1.0 m/s is shown in Fig. 4.20. The elemental analysis obtained by EDS has revealed the presence of iron and trace of oxygen on the surface and within the micro-dimples. This suggests the presence of oxides in the transfer layer due to increased frictional heating caused by increased speed.

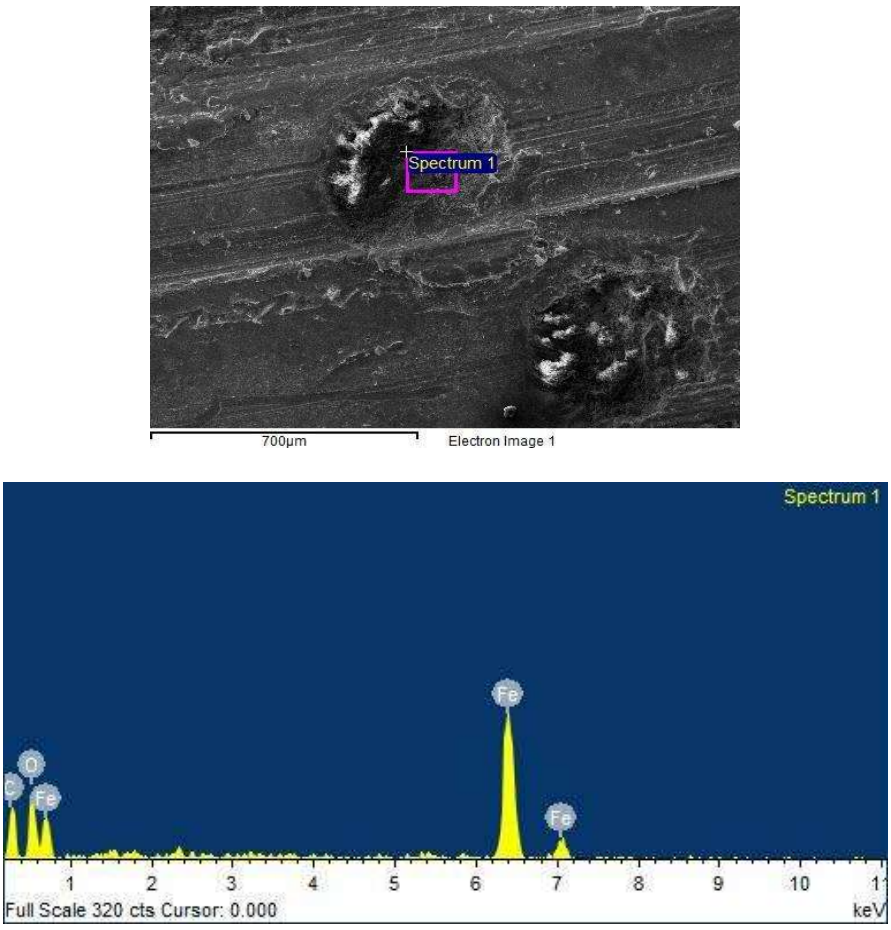

Fig. 4.20 SEM-EDS of worn surface of CT20 after sliding under the dry condition at a load of 15 N and speed of 1 m/s.

SEM-EDS depicts the worn surface of BT7 after sliding under dry conditions at a load of 30 N and a speed of 0.6 m/s, as shown in Fig. 4.21. The presence of iron and a trace of oxygen on the surface and within the micro-dimples is evident from the EDS analysis.

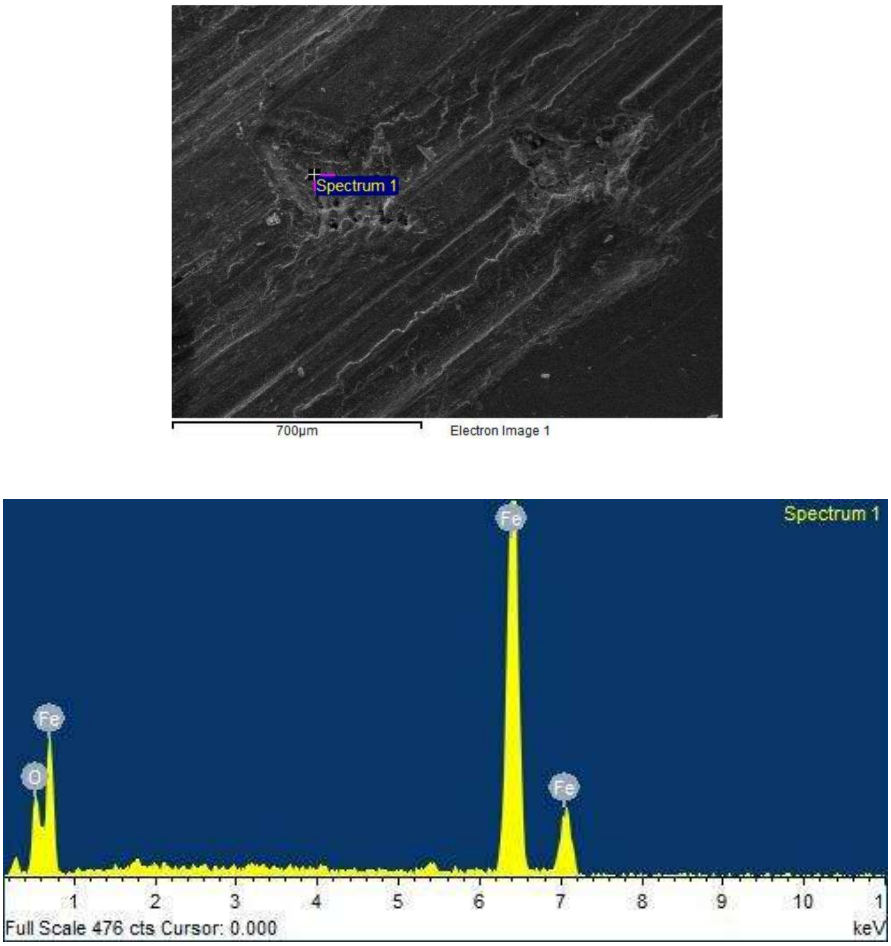

Fig. 4.21 SEM-EDS of worn surface of BT7 after sliding under the dry condition at a load of 30 N and speed of 0.6 m/s.

The optical 3D Profilometry of BT20 tested at 1m/s, and a load of 15 N is shown in Fig. 4.22. Before the test, the dimple has an average depth of about 8-10 µm, as seen in the colour bar. The high spots around the micropore are bulge on the brim. After the test, there is almost no evidence of the dimple. A worn track can be observed in the same region, along with traces of abrasive wear can be seen in Fig. 4.22 (b).

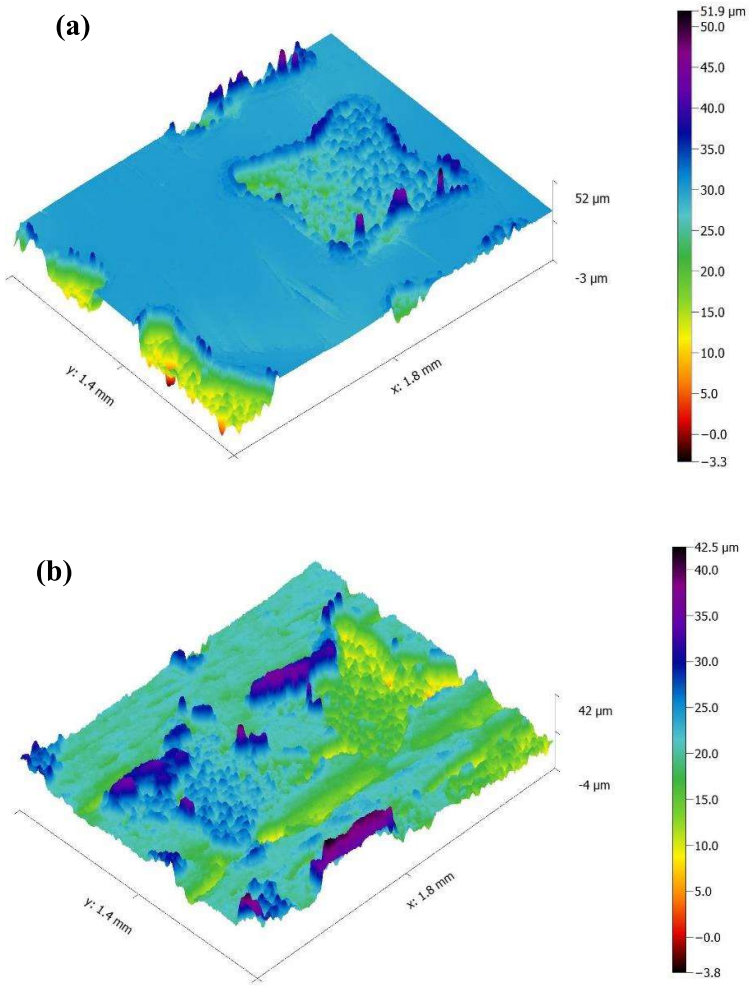

Fig. 4.22 Optical 3D Profilometry of disc surfaces before (a) and after (b) the test at a load of 15 N and speed of 1 m/s.

4.4 DISCUSSION

The observed friction and wear behaviour for the untextured steel may be explained on the basis of the adhesion between disc and counterface steel pin followed by the generation of wear debris due to relative motion. The debris either gets trapped between the sliding surfaces or may get ejected from the interface due to centrifugal forces. The debris trapped between the surface may form a compacted layer on the sliding surface and results in a reduction of both friction and wear if that gets oxidised during continued rubbing by providing

low shear strength junctions at the interface and protecting the underlying surface from direct metal to metal contact, as reported earlier also (Tyagi et al., 2002).

The increase in friction and wear in UT steel from 0.2 m/s to 0.6 m/s may be attributed to the formation of a larger number of wear particles due to a larger number of interactions per unit time, and more particles seem to have ejected as there is hardly the presence of transfer layer of the surface of this steel as observed Fig. 4.15 (a). However, the transfer layer containing oxide particles is expected to get compacted due to increased frictional heating caused by the increased speed, which provides an effective cover to the underlying substrate and reduces direct metal-metal contact leading to reduced friction and wear as reported earlier by other researchers. A decrease in the coefficient of friction for UT at 0.6 m/s at the end of the test can be observed as shown in Fig. 4.5. This may be attributed to the formation of this layer. As far as textured steels are concerned, the dimples are able to trap the wear debris particles results in a reduced wear rate in comparison to untextured steel. At the lowest speed of 0.2 m/s, the coefficient of friction is observed to decrease from UT to CT20 before increasing for BT20, as shown in Fig. 4.10, whereas the friction is found to decrease continuously from CT7 to BT20 at the highest speed. The BT20 has the lowest coefficient of friction at relatively higher speeds of 0.6 m/s and 1.0 m/s, whereas, at the lowest speed, the friction is lowest for CT20 and BT7. At a low speed of 0.2 m/s, the pin moves in contact with the disc; as speed increases to 0.6 m/s, bulges on the brim of dimples and at contact wear out, which gives the rise in coefficient of friction. As the edges are clear, these worn-out particles fill the cavity and hence give a drop in the coefficient of friction at 1m/s. A relatively lower coefficient of friction for CT20 and BT7 at a speed of 0.2 m/s may be explained on the basis of the features present on SEM micrographs presented in Fig. 4.14 (c and d), which indicate the filling of dimples by the wear debris leading to an absence of any loose debris particles which might have caused abrasion. A reduced coefficient of friction for CT20, BT7, and BT20 corresponding to a speed of 1 m/s may be

attributed to the substantial of dimples, as reflected in Fig.4.16 (c) for CT20 and complete filling of dimples for BT7 and BT20 without any visible dimples, as seen from Fig. 4.16 (d and e). This may have given rise to a smooth running as there was no loose debris available at the interface to cause abrasion resulting in a decrease in coefficient of friction. The other factor contributing to the observed behaviour may be the presence of a compacted layer of oxide caused by frictional heating, which might have provided low shearing junctions and hence, a reduced coefficient of friction. The wear rate is found to be almost the same for CT7, CT20, and BT7 at speeds of 0.2 m/s and 1.0 m/s, but BT20 has the lowest rate at 1.0 m/s, whereas, it increases slightly for 0.2 m/s. The observed behaviour may be attributed to the effectiveness of dimples in trapping the wear particles, which can be judged by an examination of worn surfaces of textured steels shown in Figs. 4.14, 4.15, and 4.16, where dimples appear to be filled to different extents depending on the test speed, shape, and density of dimples. At a relatively lower speed of 0.2 m/s, the dimples are partially filled due to less generation of loose wear debris, and hence the wear is less than observed at other speeds. As the generation of wear particles is increased with increasing speed, the dimples get completely filled (Fig. 4.16 b, c, d, and e), and the remaining debris is not able to get trapped and get ejected as loose particles, thus increasing the rate of wear. However, with a further increase in speed to 1.0 m/s, the wear rate is found to decrease again despite the filling of dimples. Under this condition, the untapped debris particles appear to have got compacted due to increased friction heating at the interface and form a compacted transfer layer (Fig. 4.16 b, c, d, and e), providing the protective cover to the underlying substrate to a varying extent leading to lower friction and wear. The elemental analysis of the worn surface obtained by SEM-EDS reveals the presence of oxygen on the surface, as evident also in the case of CT20 after sliding under the dry condition at 15 N constant load at 1.0 m/s shown in Fig. 4.20. This indicates the presence of oxide layer.

The SEM micrographs of (CT7 and BT7) at 0.2 m/s reveal that as the load increases to 30 N, the wear increases and also the margin turnup of dimples wears out and form small patches of debris (Fig. 4.17 b, d). The wear rises at 0.2 m/s as the load increases to 30 N, and the margin turnup of dimples wears off and forms small patches of debris, as seen in SEM micrographs of (CT7 and BT7). The scratches on the wear track are oriented in the sliding direction. These surface features can be explained by abrasion wear due to the presence of a third body with high mechanical properties. The dimples on the BT20 and CT20 are still visible, indicating that the existence of a larger number of dimples is more capable of entrapping the worn particles. Additionally, in comparison to circular dimples, the outward curved edges of bi-triangular dimples enable greater access for the entrapment of worn particles.

Except for CT20 and BT20, all textured specimens are filled to the point where dimples are no longer visible when the speed increases to 0.6 m/s. The dimples are less evident at the highest speed of 1 m/s and the load of 30 N employed in the study, and the bulge on the brim of the micro dimple has also vanished totally. The adhesion between the disc and the counterface steel pin, followed by the formation of wear debris owing to relative motion, can explain the observed friction and wear behaviour for untextured steel. The debris trapped between the sliding surfaces may form a compliant layer on the sliding surface that reduces friction and wear by providing low shear strength junctions at the interface and protecting the underlying surface from direct metal-to-metal contact. The decrease in friction and wear in UT steel from 0.2 m/s to 1 m/s may be attributed to the formation of a transfer layer containing oxide particles. As previously described by other researchers, these particles are projected to compact due to increased frictional heating produced by higher speed and load, which offers an effective cover to the underlying substrate and lowers direct metal-metal contact, resulting in reduced friction and wear, as observed in Figs. 4.18 (a) and 4.19 (a).

As far as textured steels are concerned, the dimples are able to trap the wear debris particles results in a reduced wear rate in comparison to untextured steel. As shown in Fig. 4.11, the coefficient of friction decreases from UT to BT20 before increasing for BT7 and CT7 at the lowest speed of 0.2 m/s. At 0.6 m/s, a similar trend is observed with a larger variation in the values for CT20 and BT20. Whereas the friction is found to decrease for textures specimens and remains closer at the highest speed. The BT20 has the lowest coefficient of friction at 0.6 m/s. At a low speed of 0.2 m/s, the pin moves in contact with the disc, and due to increased load to 30 N, bulges on the brim of dimples and at contact wear out, which gives the rise in coefficient of friction. As the edges are clear, these worn-out particles fill the cavity and hence give a drop in the coefficient of friction at 0.6 m/s. A relatively lower coefficient of friction for CT 20 and BT20 at a speed of 0.2 m/s and 0.6 m/s may be explained on the basis of a higher number of the features present, as shown in SEM micrographs in Fig. 4.17 (c and e) and 4.18 (c and e) which indicate the filling of dimples by the wear debris leading to the absence of any loose debris particles which might have caused abrasion. A reduced coefficient of friction for CT7, CT20, BT7, and BT20 corresponding to a speed of 1 m/s may be attributed to the substantial of dimples, as reflected in Fig.4.19 (c), (e) for CT20 and BT20 respectively and complete filling of dimples for CT7 and BT7 without any visible dimples, as seen from Fig. 4.16 (b and d). This may have given rise to a smooth running as no loose debris was available at the interface to cause abrasion, resulting in a decrease in the coefficient of friction. Another aspect that may have influenced this behaviour is the presence of a compact layer of oxide induced by frictional heating, which may have resulted in low shearing junctions and hence a lower coefficient of friction. The wear rate is found to be almost the same for CT20 and BT7 at speeds of 0.2 m/s and 1.0 m/s, but BT7 has the lowest rate at 1.0 m/s, whereas it increases slightly for 0.6 m/s. The wear rate is slightly more for BT20 at all the speeds when compared with BT7. The observed behaviour can be related to the effectiveness of dimples in trapping

wear particles, as seen in Figs. 4.17, 4.18, and 4.19, where dimples appear to be filled to different extents depending on the test speed, shape, and density of dimples. At a relatively lower speed of 0.2 m/s and 30 N load, generation of loose wear debris is more, also aided by wearing out of bulges, and hence the wear is more. As the generation of wear particles is increased with increasing speed, the dimples get completely filled (Fig. 4.18 b, c, d, e), and the remaining debris is not able to get trapped; however, the wear rate is found to decrease again despite the filling of dimples. Under this condition, the untapped debris particles appear to have got compacted due to increased friction heating at the interface and form a compacted transfer layer (Fig. 4.18 b, c, d, e) and (Fig. 4.19 b, c, d, e) providing the protective cover to the underlying substrate to a varying extent leading to lower friction and wear. The increased wear loss for BT20 may be due to the wearing of bulges around the brim resulting in the generation of more debris which is not able to form a compacted transfer layer and remain loose to cause abrasion of the surface.

A comparison of the friction and wear performance of circular and bi-triangular shape reflects that the bi-triangular shape is more effective in reducing both the friction and wear and that too with a relatively lower density of dimples, as evident from Figs. 4.10,11, 4.12 and 4.13. At a load of 15 N, BT7 has shown the lower coefficient of friction and wear rate, whereas at relatively higher speeds (0.6 and 1.0 m/s), BT20 has the lowest coefficient of friction and wear rate. However, at a load of 30 N, BT20 has shown the lowest coefficient of friction at all the speeds, whereas BT7 has the lowest wear rate.